Acute knockdown of Depdc5 leads to synaptic defects in mTOR-related epileptogenesis

Antonio de Fusco, Maria Sabina Cerullo, Antonella Marte, Caterina Michetti, Alessandra Romei, Enrico Castroflorio, Stéphanie Baulac, Fabio Benfenati

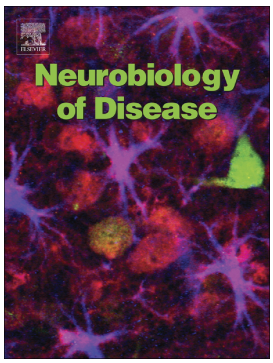

Acute knockdown of Depdc5 leads to synaptic defects in mTOR-related epileptogenesis

Antonio De Fusco, Maria Sabina Cerullo, Antonella Marte, Caterina Michetti, Alessandra Romei, Enrico Castroflorio, Stephanie Baulac, Fabio Benfenati

PII: S0969-9961(20)30097-8

DOI: https://doi.org/10.1016/j.nbd.2020.104822

Reference: YNBDI 104822

To appear in: *Neurobiology of Disease*

Received date: 13 November 2019

Revised date: 2 February 2020

Accepted date: 26 February 2020

Please cite this article as: A. De Fusco, M.S. Cerullo, A. Marte, et al., Acute knockdown of Depdc5 leads to synaptic defects in mTOR-related epileptogenesis, *Neurobiology of Disease*(2020), https://doi.org/10.1016/j.nbd.2020.104822

Neurobiology of Disease
NBD-19-1245
2nd revised version

Acute knockdown of Depdc5 leads to synaptic defects in mTOR-related epileptogenesis

Antonio De Fusco[1,2,#], Maria Sabina Cerullo[1,2,#], Antonella Marte[2,3], Caterina Michetti[1,3], Alessandra Romei[1,2], Enrico Castroflorio[1,*], Stephanie Baulac[4] and Fabio Benfenati[1,3]

[1]Center for Synaptic Neuroscience and Technology, Istituto Italiano di Tecnologia, Largo Rosanna Benzi 10, 16132 Genova, Italy
[2]Department of Experimental Medicine, University of Genova, Viale Benedetto XV, 3, 16132 Genova, Italy
[3]IRCSS, Ospedale Policlinico San Martino, Largo Rosanna Benzi 10, 16132 Genova, Italy
[4] Sorbonne Université, UPMC Univ Paris 06, UMR S 1127; INSERM, U1127; CNRS, UMR 7225; Institut du Cerveau et de la Moelle épinière (ICM), Hôpital Pitié-Salpêtrière, F-75013, Paris, France

[#]Equal contribution
*Present address: MRC Harwell Institute, Harwell Campus, Oxfordshire, OX11 0RD, UK.

Correspondence should be sent to:
Fabio Benfenati, MD
Center for Synaptic Neuroscience and Technology
Istituto Italiano di Tecnologia
Largo Rosanna Benzi 10
16132 Genova, Italy
phone +39 010 71781434
fax +39 010 3538194
email fabio.benfenati@iit.it

Abstract

DEP-domain containing 5 (DEPDC5) is part of the GATOR1 complex that functions as key inhibitor of the mechanistic target of rapamycin complex 1 (mTORC1). Loss-of-function mutations in *DEPDC5* leading to mTOR hyperactivation have been identified as the most common cause of either lesional or non-lesional focal epilepsy. However, the precise mechanisms by which *DEPDC5* loss-of-function triggers neuronal and network hyperexcitability are still unclear. In this study, we investigated the cellular mechanisms of hyperexcitability by comparing the constitutive heterozygous Depdc5 knockout mouse *versus* different levels of acute Depdc5 deletion (≈40% and ≈80% neuronal knockdown of Depdc5 protein) by RNA interference in primary cortical cultures. While heterozygous *Depdc5*$^{+/-}$ neurons have only a subtle phenotype, acutely knocked-down neurons exhibit a strong dose-dependent phenotype characterized by mTOR hyperactivation, increased soma size, dendritic arborization, excitatory synaptic transmission and intrinsic excitability. The robust synaptic phenotype resulting from the acute knockdown Depdc5 deficiency highlights the importance of the temporal dynamics of Depdc5 knockdown in triggering the phenotypic changes, reminiscent of the somatic second-hit mechanism in patients with focal cortical dysplasia. These findings uncover a novel synaptic phenotype that is causally linked to *Depdc5* knockdown, highlighting the developmental role of Depdc5. Interestingly, the synaptic defect appears to affect only excitatory synapses, while inhibitory synapses develop normally. The increased frequency and amplitude of mEPSCs, paralleled by increased density of excitatory synapses and expression of glutamate receptors, may generate an excitation/inhibition imbalance that triggers epileptogenesis.

Keywords: Depdc5, mTOR pathway, knockdown, synapses, RNA interference, heterozygous mice, epilepsy, focal cortical dysplasia

Highlights:

- ✓ Acute *Depdc5* knockdown leads to a robust neuronal and synaptic phenotype
- ✓ *Depdc5* knockdown increases neuronal soma size and dendritic arborization
- ✓ *Depdc5* knockdown alters synaptic connectivity
- ✓ *Depdc5* knockdown induces an excitation/inhibition imbalance at the synaptic level
- ✓ The hyperexcitability of excitatory neurons further increases excitatory strength

Introduction

Mutations in the *DEPDC5* (Disheveled, Egl-10 and Pleckstrin (DEP) domain-containing protein 5)[1] gene have been identified as the most common cause of either lesional or non-lesional focal epilepsy (Dibbens et al., 2013; Ishida et al., 2013; Baldassari et al., 2019a). In patients, brain magnetic resonance imaging and neuropathology have disclosed a spectrum of Malformations of Cortical Development, ranging from Focal Cortical Dysplasia (FCD) to subtle band heterotopias (Scheffer et al., 2014; Baulac et al., 2015; D'Gama et al., 2017; Baldassari et al., 2019a).

Physiologically, DEPDC5 is a member of the GAP Activity Toward Rags complex 1 (GATOR1) which also comprises the nitrogen permease regulator-like 2 and 3 (NPRL2 and NPRL3). GATOR1 represents a key component of the amino acid-sensing branch of the mTOR pathway, inhibiting the mTOR complex 1 (mTORC1; Bar-Peled et al., 2013). In neurons, mTORC1 is involved in regulating neuronal metabolism, growth and homeostasis, and plays a key role in neuronal differentiation, neurite outgrowth and synaptic formation during neuronal development (Laplante and Sabatini, 2012; Lasarge and Danzer, 2014; Bockaert and Marin, 2015).

While the constitutive deletion of *Depdc5* is embryonically lethal, heterozygous *Depdc5* rats and mice failed to recapitulate the major traits of the human disease (Marsan et al., 2016; Hughes et al., 2017). Indeed, both *Depdc5*$^{+/-}$ mice and rats did not display spontaneous seizures or increased propensity to epileptic seizures triggered by a single dose of pentylenetetrazol (Marsan et al., 2016; Hughes et al., 2017). However, *Depdc5*$^{+/-}$ rats exhibited a mild phenotype with dysmorphic pyramidal neurons and altered cortical excitability (Marsan et al., 2016). Interestingly, a neuron-specific *Depdc5* knockout mouse displayed a progressive neuronal phenotype with macrocephaly, dysmorphic neurons and increased susceptibility to spontaneous and provoked seizures (Yuskaitis et al., 2018). A morpholino oligonucleotide-mediated *Depdc5* knockdown in the zebrafish was also characterized by motor hyperactivity and increased neuronal activity (de Calbiac et al., 2018), while a zebrafish full knockout model showed spontaneous epileptiform events, increased seizure propensity a premature death that were associated with defects in GABAergic networks (Swaminathan et al., 2018). At the cellular level, shRNA-mediated *Depdc5* or *Nprl3* knockdown in mouse neuroblastoma cells or in mouse neural progenitors derived from the subventricular zone

[1] AZ, active zone; DEPDC5, Disheveled, Egl-10 and Pleckstrin domain-containing protein 5; FCD, Focal Cortical Dysplasia; GATOR1, GAP Activity Toward Rags complex 1; MOI, multiplicity of infection; mEPSC, miniature excitatory postsynaptic current; mIPSC, miniature inhibitory postsynaptic current; mTORC1, mTOR complex 1; NeuN, neuronal nuclear antigen; NGS, normal goat serum; Nprl, nitrogen permease regulator-like; PB, phosphate buffer; PBS, phosphate buffered saline; pS6, phosphorylated S6; PTZ, pentylenetetrazol; qRT-PCR, quantitative Real-Time Polymerase Chain Reaction; RT, room temperature; Scr, scramble; sh, short hairpin; SV, synaptic vesicle; Ta, annealing temperature; tGFP, turbo-Green Fluorescent Protein; TEM, transmission electron microscopy; TTX, tetrodotoxin; vGAT, vesicular GABA transporter; vGlut1, vesicular glutamate transporter-1.

induced mTOR hyperactivation causing soma enlargement, increased filopodia formation and mislocalization of mTOR at lysosomes in the absence of amino acids (Iffland et al., 2018).

Recently, the combination of in utero electroporation with the CRISPR/Cas9 technology succeeded in creating focal somatic *Depdc5* deletions in the mouse embryonic brain. These models recapitulate the main clinical and neuropathological features of *DEPDC5* patients, with the presence of dysmorphic and ectopic pyramidal neurons, cortical layering abnormalities, spontaneous seizures, and premature sudden death due to terminal seizures (Ribierre et al., 2018; Hu et al., 2018). A recently generated conditional *Depdc5* mouse resulted in mTORC1 hyperactivity, decreased thresholds to PTZ-induced seizures and FCD-like phenotype (Dawson et al., 2019). These studies support the prospect that the most severe human DEPDC5-linked phenotypes (i.e. with an FCD) are due to a "double-hit" germline and somatic mosaic inactivation of *DEPDC5*. Although it is clear that mTOR hyperactivity caused by loss-of-function *DEPDC5* mutations impacts brain morphogenesis and development, the epileptogenic mechanisms occurring at the cellular levels are still largely unknown, particularly regarding the morphological and functional impact of DEPDC5 deficiency at level of synaptic connectivity and transmission.

To investigate the neuronal and synaptic effects consequences of the acute DEPDC5 knockdown by somatic mutations and compare it with the corresponding phenotype of constitutive heterozygous Depdc5 deficiency, we induced various levels of acute *Depdc5* knockdown in wild type primary neurons by RNA interference. While heterozygous *Depdc5*$^{+/-}$ neurons display a subtle phenotype, the more effective *Depdc5* knockdown by RNA interference (*Depdc5*^{KD1}) triggers a much stronger phenotype of mTOR hyperactivation associated with increased excitatory synaptic transmission and intrinsic excitability of excitatory neurons. The synaptic phenotype resulting from the acute Depdc5 deficiency by RNA interference suggests an important developmental role of *Depdc5* that can be causally related to epileptogenesis.

Materials and methods

Experimental animals. Heterozygous *Depdc5* KO mice (C57BL/6N background) were obtained from the IMPC European Consortium at the Sanger Institute (UK) within the European EMMA/Infrafrontier initiative and bred at the IIT SPF animal facility. The EUCOMM/KOMP targeting strategy was based on the "*knockout-first allele*" (Tm1a) designed to be a knockout by splicing the cDNA to a LacZ cassette. The cassette was then inserted into the intronic region upstream the critical exon 5 of the *Depdc5* locus to create a null allele of the gene (Skarnes et al., 2011). Genotyping was performed by PCR with the following primers *Depdc5*_F: GGTTTTAGTTTTTGGATTTGTTTCA, *Depdc5*_R: GCCTTTAATCCCAGCACTTG; 5mut-R1_Term: GAACTTCGGAATAGGAACTTCG, that were used to detect the WT (+/+) (*Depdc5*_F plus *Depdc5*_R product, 227 bp) and mutant (*Depdc5*_F plus CAS_R1_Termproduct, 129 bp) *Depdc5* alleles and to genotype wild type (WT; +/+) and heterozygous (+/-) mice. The colony was maintained on a C57BL/6N background and propagated in heterozygosity. Two females were housed with one male in standard Plexiglas cages (33 × 13 cm), with sawdust bedding and a metal top. After two weeks of mating, male mice were withdrawn and dams were housed individually and daily checked for delivery. Mice were maintained on a 12:12 h light/dark cycle (lights on at 7 a.m.) at constant temperature (21 ± 1 °C) and relative humidity (60 ± 10 %). Animals were provided drinking water and a complete pellet diet (Mucedola, Settimo Milanese, Italy) *ad libitum*. Mouse genotypes were determined at weaning (P20-25) by RT-PCR on tail samples. Mice were weaned into cages of same sex pairs. Sample mice of both genotypes were video recorded and inspected offline to monitor spontaneous behavioral seizures.

Wild type C57BL/6J mice were used as a source of primary neurons for the RNA interference experiments. All experiments were carried out in accordance with the guidelines established by the European Communities Council (Directive 2010/63/EU of March 4th, 2014) and were approved by the local Ethics Committee and the Italian Ministry of Health (authorization n. 1276/2015-PR).

immunohistochemistry. Depdc5$^{+/+}$ and *Depdc5*$^{+/-}$ littermates (3-4 months of age) were deeply anesthetized with an intraperitoneal injection of urethane and transcardially perfused with ice-cold 0.1 M phosphate buffer (PB; pH 7.4), followed by 4% paraformaldehyde in 0.1 PB. After perfusion, brains were briefly dissected and post-fixed in the same fixative solution overnight at 4 °C. After several washes in 0.1 M PB, brains were then cryoprotected by immersion in 10, 20 and 30% sucrose solutions and subsequently cut in 30 µm sections with a Vibratome and stored at − 20 °C in a solution containing 30% ethylene glycol and 20% glycerol in 0.1 M PB. Sections containing frontal and somatosensory cortex were then washed in phosphate-buffered saline (PBS, pH 7.4) and processed for free-floating immunofluorescence. After blocking step in PBS containing 0.05% Triton X-100 and 10% normal goat serum (NGS), sections were incubated overnight at room

temperature (RT) with the following primary antibodies: rabbit anti-vesicular GABA transporter (vGAT; 1:250, Synaptic System), guinea pig anti-vesicular glutamate transporter-1 (vGlut1; 1:250, Synaptic System), rabbit anti-phosphorylated $S6^{240-244}$ (pS6; 1:250, Synaptic System) or mouse anti-neuronal nuclear antigen (NeuN; 1:5000, Cell Signaling). Antibodies were diluted in PBS with 3% of NGS and 0.05% Triton X-100. Double immunofluorescence (pS6-NeuN or vGlut1/vGAT) was performed with the simultaneous addition of the primary antibodies. Sections were then washed in PBS (4 × 10 min) and incubated for 1 h at 25 °C with anti-rabbit Alexa Fluor 488, and anti-mouse Alexa Fluor 568 or anti-guinea pig Alexa Fluor 488 (Invitrogen). After several PBS rinses, sections were mounted on glass slide and observed with a Leica SP8 confocal microscope (Leica Microsystem). Z-series stacks of seven consecutive confocal sections (1024x1024 pixels) for a total depth of 2 µm of tissue were acquired at 20 x using the multi-track mode to avoid fluorescence crosstalk (pinhole: 1.0 airy unit) and background labeling was subtracted. Sections of frontal or somatosensory cortices were reconstructed and analyzed using ImageJ. Cortical layers were defined based on neuronal morphology and distribution from the NeuN stained sections as follows: Layer I includes only a few nerve cells; Layer II/III consists of numerous and densely packed small and medium-sized pyramidal neurons; Layer IV contains small, irregularly shaped nerve cells; Layer V includes large pyramidal neurons; Layer VI is characterized by small polymorphic and fusiform nerve cells. For the analysis of the vGlut/vGAT ratio, the whole cortical layers were reconstructed offline, then each channel was thresholded to remove background staining and the number of puncta was counted by mean of ImageJ software automatic feature. The analysis was done by an experimenter blind to the genotype.

RNA extraction, retrotranscription and qRT-PCR. Total cellular or tissue RNA was extracted using TRIzol (Life Technologies). RNA concentration was quantified by using theNanodrop-1000 spectrophotometer (Thermo Scientific). cDNA was synthesized starting from 0.25 µg RNA with SuperScript IV Reverse Transcriptase kit (#18090010; Thermo Fisher) according to manufacturer's instruction and used for qRT-PCR. Gene expression was measured by quantitative real-time PCR using C1000 Touch™ Thermal Cycler (Bio-Rad) on a CFX96™Real-Time System following the manufacturer's protocol. Real time PCR analyses were performed using the SYBR Green I Master mix (Roche), on a Lightcycler 480 (Roche), with the following protocol: 95 °C for 5 min; 10s at 95 °C / 20 s at the specific annealing temperature (Ta) / 10 s at 72 °C for 45 cycles; melting curve (heating ramp from 55 °C to 95 °C) in order to check for amplification specificity. The following primers (final concentration 0.25 µM) and annealing temperature were used:

*Depdc5*_F: TGATGCCTACGATGCTCAAG, Ta= 64 °C;

*Depdc5*_R: TGGCTCCTCACTTCCTCAGT, Ta= 64.1 °C;

*Gapdh*_F: GATCATCAGCAATGCCTCCT, Ta= 59.8 °C;

*Gapdh*_R: TGTGGTCATGAGTCCTTCCA, Ta= 61.7 °C;

Relative gene expression was determined using the ΔΔCT method, normalizing data the housekeeping transcript (*Gapdh*).

Pentylenetetrazol-induced seizures. *Depdc5*$^{+/+}$ and *Depdc5*$^{+/-}$ littermates (3-4 months of age) were repeatedly injected with unitary doses of pentylenetetrazol (PTZ; 10 mg/kg intraperitoneally in 0.9% saline) every 10 min and continuously monitored after each injection in a 17x17x25 cm box equipped with the AnyMaze video tracking system. Seizure scoring was conducted as previously reported by Browning and Nelson (1986), and the following parameters were considered: (i) myoclonic jerk, (ii) face and forelimb clonus (iii) whole body clonus with twisting or loss of posture, (iv) running/bouncing clonus, (v) tonus: (tonic flexion and tonic extension). At the end of the observation period, animals were euthanized humanely by cervical dislocation. Seizure manifestations were recorded by inspection of the videos by two independent observers blind to the genotype. Seizure threshold was defined as the dose (mg/kg) necessary to induce a score (v).

Plasmids and viral vectors. Four distinct short hairpin (sh) RNAs (Origene, TL508165) and a non-effective 29-mer scrambled shRNA (Scr) construct (Origene, TR30021) in a pGFP-C-Lenti vector were used to acutely silence *Depdc5* expression. Sequences were:
sh1: AAGTGAGGAGCCAGGCTTCTGATGACACG
sh2: GTGGACCAGACTGTGACTCAAGTATTCCG
sh3: TGTCCGACCTGGAGGATACACGCCTCAGA
sh4: CTCCAGTCGGCAAGAAAGGAACCTCAGCT
Scr: GCACTACCAGAGCTAACTCAGATAGTACT
As a control for viral transduction, the empty lentiviral construct pCCL-sin-PPT-prom-EGFP-Wpre (kindly provided by Dr. M. Amendola, Telethon Institute for Gene Therapy) was used. Lentiviral particles encoding these vectors are a modification of Addgene plasmids 8454, 8455 co-expressing turbo-Green Fluorescent Protein (tGFP) as a reporter and were produced as previously described (Stewart et al., 2003) at the Virus Core Facility, Charité University, (Berlin, Germany) or were produced at NSYN viral facility as previously described (De Palma and Naldini, 2002).

Culture and transfection of cell lines. HEK-T293 cells were cultured in Dulbecco's MEM (DMEM; Gibco) supplemented with 10% fetal calf serum (Gibco), 1% L-glutamine, 100 U/ml penicillin, and 100 µg/ml streptomycin (Gibco) and maintained at 37 °C in a 5% CO^2 humidified atmosphere. For transfection experiments Lipofectamin2000 (Thermo Scientific) was used according to the manufacturer's protocol, and cells were incubated under standard growth conditions for 72 h and then processed.

Cultures and transduction of primary neurons. Low-density cortical neurons were prepared from WT C57BL/6J (Charles River) for RNA interference experiments or from *Depdc5*$^{+/+}$ and *Depdc5*$^{+/-}$ C57BL/6N mice, as previously described (Baldelli et al. 2007; Chiappalone et al. 2009). Animals were sacrificed by CO_2 inhalation and 17/18-day embryos (E17-18) were immediately removed by cesarean section. In brief, cerebral cortices were dissociated by enzymatic digestion in 0.125% trypsin for 20 min at 37 °C and then triturated with a fire-polished Pasteur pipette. Primary cultures of dissociated cortical neurons were subsequently plated onto poly-D-lysine (0.1 mg/ml, Sigma-Aldrich)-coated 25-mm glass coverslips ($6x10^4$ cells/coverslip) and 35-mm wells (1×10^6 cells/well). Neurons were maintained in a culture medium consisting of Neurobasal (Gibco) supplemented with B27 (1:50 v/v, Gibco), Glutamax (1% w/v, Gibco), penicillin–streptomycin (1%, Gibco) and kept at 37 °C in a 5% CO_2 humidified atmosphere. For shRNA transfection experiments, neurons ($4x10^6$) were nucleofected before with Amaxa basal nucleofector kit for primary neurons (Lonza) with 4 µg of plasmid DNA according to the manufacturer's protocol or underwent the same procedure without plasmid DNA (control neurons). For lentiviral transduction experiments, 7 DIV cortical neurons were infected with lentiviruses at 10 multiplicity of infection (MOI). After 24 h, the medium was replaced with an equal volume of fresh and conditioned medium (1:1). All experiments were performed 5-6 days post-infection, when not differently indicated. Transduction efficiency was always above 75% of neuronal cells.

Western blotting. Total cell lysates were obtained from cortical neuronal cultures or whole brains from E12.4 mouse embryos. Cells were extracted in lysis buffer (150 mM NaCl, 50 mM Tris-HCl pH 7.4, 1 mM EDTA, 1% Triton X-100) supplemented with protease and phosphatase inhibitor cocktails (Roche, Monza, Italy). After 10 min of incubation on ice, cell lysates were collected and clarified by centrifugation (10 min at 10,000 x g at 4 °C). Brains were dissected and pottered in liquid nitrogen, then centrifuged at 1,000 x g for 10 min at 4 °C. Protein concentration was determined using BCA (Thermo Scientific) assay. Equivalent amounts of protein were subjected to SDS-PAGE on 10% polyacrylamide gels and blotted onto nitrocellulose membranes (Whatman). Blotted membranes were blocked for 1 h in 5% milk in Tris-buffered saline (10 mM Tris, 150 mM NaCl, pH 8.0) plus 0.1% Triton X-100 and incubated overnight at 4 °C with the following primary antibodies: rabbit anti-Depdc5 (1:1000, Abcam ab185565), rabbit anti-phosphorylated S6 protein (1:2000, Sigma-Aldrich #5364), mouse anti-S6 (1:1000, Synaptic Systems #2317) and mouse anti-actin (1:2000, Sigma-Aldrich A2228). Membranes were washed and incubated for 1 h at RT with peroxidase-conjugated goat anti-mouse (1:3000; Bio-Rad) or anti-rabbit (1:5000; Bio-Rad) antibodies. Bands were revealed with the ECL chemiluminescence detection system (Thermo Scientific) and the quantification of immunoreactivity was performed by densitometric analysis of the fluorograms by building a standard curve with increasing protein amounts of the starting

material and interpolating the optical density of the unknown samples into the linear part of the standard curve over various exposure times.

Patch-clamp recording in primary cortical neurons. Whole patch-clamp recording were made from primary cortical neurons as previously described (Baldelli et al. 2007; Chiappalone et al. 2009) using a Multiclamp 700B/Digidata1440A system (Molecular Devices, Sunnyvale, CA). Patch pipettes, prepared from thin borosilicate glass, were pulled and fire-polished to a final resistance of 4-5 MΩ when filled with standard internal solution. For all the experiments, cells were maintained in standard extracellular Tyrode solution containing (in mM): 140 NaCl, 2 $CaCl_2$, 1 $MgCl_2$, 4 KCl, 10 glucose, and 10 HEPES (pH 7.3 with NaOH). For the analysis of neuronal excitability, D-(−)-2-amino-5-phosphonopentanoic acid (D-AP5; 50 µM), 6-cyano-7 nitroquinoxaline-2,3-dione (CNQX; 10 µM), bicuculline methiodide (30 µM), and (2S)-3-[[(1S)-1-(3,4-dichlorophenyl)ethyl]amino-2-hydroxypropyl] (phenylmethyl)phosphinic acid hydrochloride (CGP58845; 5 µM) were added to block NMDA, non-NMDA, $GABA_A$, and $GABA_B$ receptors, respectively. Current-clamp recordings of AP firing activity were performed at a holding potential of −70 mV and APs were induced by injection of 10 pA current steps lasting 500 ms in morphologically identified pyramidal neurons. Excitatory neurons were identified by estimating the AP failure ratio evoked by short trains of high-current steps at increasing frequency (10-120 Hz; Prestigio et al., 2019). The mean firing frequency was calculated as the number of APs evoked by minimal current injection in 500 ms, whereas the instantaneous frequency was estimated as the reciprocal value of the time difference between the first two evoked APs. Current-clamp recordings of APs were acquired at a 50 kHz and filtered at 1/5 of the acquisition rate with a low-pass Bessel filter. The mean firing frequency and the instantaneous frequency were analyzed using Clampfit 10.7 (Molecular Devices, Sunnyvale, CA) and Prism softwares. The shape properties of the first AP elicited by minimal current injection were analyzed by building time-derivatives of voltage (dV/dt) *versus* voltage plots (phase-plane plots) as previously described (Valente et al., 2016; Prestigio et al., 2019). Phase-plane plots were obtained and analyzed with the software OriginPro-8 (OriginLab Corp., Northhampton, MA, USA). For recording miniature excitatory postsynaptic currents (mEPSCs), bicuculline, CGP58845, D-AP5 and tetrodotoxin (TTX; 300 nM) were added to the extracellular solution to block $GABA_A$, $GABA_B$, NMDA receptors and generation and propagation of spontaneous action potentials (APs). For miniature Inhibitory Postsynaptic Currents (mIPSCs), D-AP5, CGP58845, CNQX and TTX (300 nM) were added in the Tyrode extracellular solution. The internal solution (K-gluconate) used for recording APs in current-clamp and mEPSCs in voltage-clamp configuration contained (in mM): 126 K gluconate, 4 NaCl, 1 $MgSO_4$, 0.02 $CaCl_2$, 0.1 BAPTA, 15 glucose, 5 Hepes, 3 ATP, and 0.1 GTP (pH 7.3 with KOH). The internal solution (KCl) used for mIPSC recordings contained (in mM): 126 KCl, 4 NaCl, 1 $MgSO_4$, 0.02 $CaCl_2$, 0.1 BAPTA, 15 glucose, 5 Hepes, 3 ATP, and 0.1 GTP (pH 7.3 with KOH). All the reagents were from Tocris, otherwise specified. Both mEPSCs and mIPSCs

were acquired at a 10 kHz sample frequency and filtered at 1/5 of the acquisition rate with a low-pass Bessel filter. The amplitude and frequency of the miniature excitatory and inhibitory events were calculated using a peak detector function using appropriate threshold amplitudes and areas. The frequency, amplitude and kinetics of miniature PSCs were analyzed using the MiniAnalysis (Synaptosoft) and Prism (GraphPad Software, Inc.) softwares. All experiments were performed at RT.

Immunocytochemistry. Primary cortical neurons were fixed in 4% formaldehyde, freshly prepared from paraformaldehyde, in 0.1 M PB, pH 7.4 for 20 min at RT and immunostained for specific pre/postsynaptic markers of excitatory and inhibitory synapses. Briefly, after several washes in PBS, cells were permeabilized and blocked for 30 min in 0.05% Triton X-100 and 10% normal goat serum (NGS) in PBS and then incubated overnight with primary antibodies diluted in 3% NGS and 0.05% Triton X-100 in PBS. Antibodies were used as follows: rabbit anti-phosphorylated-S6 protein (Cell Signaling, #2215), guinea pig anti-vGlut1 (1:500, Synaptic Systems, 135 304), mouse anti-Homer1 (1:200; Synaptic Systems, 160 011), rabbit anti-vGAT (1:500; Synaptic Systems 131 003), mouse anti-Gephyrin (1:500; 147 011), rabbit anti-GluA1 (1:500; Synaptic Systems, 182 003), rabbit anti-$GABA_A$-β2 receptor subunit (1:500; Synaptic Systems, 224 803). Neurons were then washed three times in PBS and then incubated in the same buffer with Alexa-conjugated secondary antibodies (1:1500, Invitrogen) and counterstained with Hoechst for nuclei detection. After several washes in PBS, coverslips were mounted with Moviol mounting medium. Images were acquired using a 40x objective with a Leica SP8 confocal microscopy (Leica Microsystems, Wetzlar, Germany). Images were processed using the colocalization plugin of ImageJ. For the analysis of synaptic density, basal dendrites of neurons were considered, and the colocalization analysis was performed, after threshold subtraction, to evaluate the simultaneous presence of pre- and a post-synaptic markers (-vGlut1/Homer1 for excitatory synapses and vGAT/Gephyrin for inhibitory synapses). For experiments with transduced neurons, only tGFP-positive neurons were analyzed. To identify *bona fide* synaptic boutons, we selected colocalized puncta within an area of 0.1-1 μm^2, corresponding to the overlapping area of pre- and post-synaptic proteins. We counted the number of synaptic puncta present within 30 µm dendrite tracts starting from the cell body. For the analysis of postsynaptic receptors, the thresholded signal of Homer1 and Gephyrin was overlapped to GluA1 and $GABA_A$-β2 receptors, respectively, and the fluorescence intensity was measured only within this colocalization area. Data are referred to three independent experiments carried out in duplicate with 5-10 neurons analyzed per duplicate.

Electron Microscopy. Low-density cultures of cortical neurons from *Depdc5*$^{+/+}$ and *Depdc5*$^{+/-}$ embryos, or from WT C57BL/6J embryos infected at 7 DIV with either shScr or sh*Depdc5* lentiviruses were processed for transmission electron microscopy (TEM). Neurons were fixed at

14-15 DIV with 1.2% glutaraldehyde in 66 mM sodium cacodylate buffer, post-fixed in 1% OsO_4, 1.5% $K_4Fe(CN)_6$, 0.1 M sodium cacodylate, *en bloc* stained with 10% of uranyl acetate replacement stain (EMS) for 30 min, dehydrated, and flat embedded in epoxy resin (Epon 812, TAAB). After baking for 48 h, the glass coverslips were removed from the Epon block by thermal shock and neurons were identified by means of a stereomicroscope. Embedded neurons were excised from the block and mounted on a cured Epon block for sectioning using an EM UC6 ultramicrotome (Leica Microsystems). Ultrathin sections (60-70 nm thick) were collected on 200-mesh copper grids (EMS) and observed with a JEM-1011 electron microscope (Jeol, Tokyo, Japan) operating at 100 kV using an ORIUS SC1000 CCD camera (Gatan, Pleasanton, CA). For each experimental condition, at least 30 images of synapses were acquired at 10,000x magnification (sampled area per experimental condition: 36 µm²). Synaptic vesicles (SVs) were defined as spherical organelles with a diameter of approximately 40 nm. Synaptic morphological features, including nerve terminal area, active zone (AZ) length, number and density of total SVs and of AZ-docked SVs were determined using ImageJ.

Statistical analysis. Data are expressed as means + SEM or box plot showing median, mean, 25th to 75th interquartile range and min to max values for number of cells (N) or independent preparations as detailed in the figure legends. Normal distribution of data was assessed using the D'Agostino-Pearson's normality test (n>6) or the Shapiro-Wilk test (n≤6). The F-test was used to compare variance between two sample groups. To compare two experimental groups, either the two-tailed unpaired Student's *t*-test or the non-parametric Mann-Whitney's *U*-test was used based on data distribution. To compare more than two normally distributed experimental groups, one-way ANOVA (followed by the Bonferroni's multiple comparison test) or repeated measures ANOVA was used. To compare more than two experimental groups that are not normally distributed, the Kruskal-Wallis ANOVA was used, followed by the Dunn's multiple comparison test. Significance level was preset to $p<0.05$. Statistical analysis was carried out using Prism (GraphPad Software, Inc., La Jolla, CA).

Results

Generation of Depdc5-deficient models

To evaluate the loss of *Depdc5* gene expression obtained by the insertion of the Tm1a allele (**Fig. 1A**; see Materials and Methods), we performed qRT-PCR and western blotting in whole brains of E12.5 *Depdc5*$^{+/+}$, *Depdc5*$^{+/-}$ and *Depdc5*$^{-/-}$ mouse embryos to determine mRNA and protein levels of Depdc5, respectively (**Fig. 1B,C**). As previously assessed in other murine models of constitutive Depdc5 knockout (Marsan et al., 2016; Hughes et al., 2017), homozygous deletion of *Depdc5* was associated with prenatal mortality in 100% of the litters, as *Depdc5*$^{-/-}$ E17 embryos or newborns were never observed. Quantitative RT-PCR analysis confirmed that *Depdc5* mRNA levels were significantly reduced in *Depdc5*$^{+/-}$ and *Depdc5*$^{-/-}$ embryos by ≈ 50% and ≈ 90%, respectively, compared to *Depdc5*$^{+/+}$ littermates (**Fig. 1B;** p=0.0016, one-way ANOVA/Bonferroni's tests), while Depdc5 protein levels were reduced of ≈ 50% and ≈ 100% respectively (**Fig. 1C**; p=0.002, one-way ANOVA/Bonferroni's tests). Although traces of *Depdc5* mRNA were detected by qRT-PCR, the total absence of Depdc5 protein in *Depdc5*$^{-/-}$ embryos indicates that the Tm1a allele efficiency is ~100%, as the residual transcript does not lead to any detectable protein translation.

To assess the effects of acute Depdc5 deficiency in primary neurons, we adopted an RNA interference strategy and designed four anti-*Depdc5* shRNA constructs (sh1-sh4) targeting distinct coding regions of the *Depdc5* mRNA (**Fig. S1A**). The scrambled and the 4 shRNA constructs were first independently transfected in HEK-293T cells and the resulting *Depdc5* transcript levels were evaluated by qRT-PCR analysis. All shRNAs significantly reduced *Depdc5* mRNA levels compared to the scrambled construct, with the most intense *Depdc5* mRNA down-regulation induced by sh3 (≈70% decrease; p=0.008, Kruskal-Wallis ANOVA/Dunn's tests; **Fig. S1B**). For subsequent experiments, we chose the sh3 construct to produce an intense knockdown of Depdc5, and the sh4 construct to model a milder knockdown and validate the knockdown specificity. We next transduced primary cortical neurons with lentiviral vectors encoding for sh3 (*Depdc5*^{KD1}), sh4 (*Depdc5*^{KD2}) or a scramble construct (*Depdc5*^{Scr}). We found that *Depdc5*^{KD1} and *Depdc5*^{KD2} neurons exhibited significant ≈80% and ≈45% reductions in *Depdc5* mRNA levels, respectively, compared to *Depdc5*^{Scr} (p=0.0007 and p=0.028 Student's *t*-test/Mann-Whitney's *U*-test; **Fig. 1D,F**). Western blot analysis confirmed that, a parallel and significant reduction in the levels of Depdc5 protein (≈80% and ≈40% reduction, respectively) also occurred in *Depdc5*^{KD1} and *Depdc5*^{KD2} neurons (**Fig. 1E,G**; p=0.045 and p=0.028, Student's *t*-test/Mann-Whitney's *U*-test).

Altered cortical synaptic connectivity in *Depdc5*$^{+/-}$ mice is associated with lower seizure thresholds

Given the importance of *DEPDC5* mutations in FCD etiology (Baulac et al., 2015; Baldassari et al., 2019a,b), we checked for the presence of subtle alterations in cortical architecture in *Depdc5*$^{+/-}$

mice. We found that heterozygous mice had a significantly increased number of pS6-positive neurons in cortical sections from frontal (p=0.0006, Mann-Whitney's *U*-test) and somatosensory (p=0.005, Mann-Whitney's *U*-test) cortices, suggesting mTOR hyperactivity (**Fig. 2A,B**)**.** However, when we measured the total cortical thickness, as well as single layer thickness in slices stained with the Neuronal Nuclear Marker (NeuN), no significant differences between *Depdc5*$^{+/+}$ and *Depdc5*$^{+/-}$ mice were detected (**Fig. S2**), ruling out an overt disturbance in the central nervous system development.

We then assessed whether *Depdc5*$^{+/-}$ mice displayed any excitatory/inhibitory imbalance in synaptic connectivity by counting, in cortical sections, puncta positive for vGlut1 and vGAT that are presynaptic markers of excitatory and inhibitory synapses, respectively. Interestingly, *Depdc5*$^{+/-}$ mice showed an increased vGlut1/vGAT ratio in both frontal and somatosensory regions (p=0.042 and p=0.01, respectively, Student's *t*-test; **Fig. 2C,D**), opening the possibility of an increased epileptic propensity.

Adult (3-4 months old) *Depdc5*$^{+/-}$ mice did not display spontaneous behavioral tonic-clonic seizures, as assessed by long-term video monitoring. However, when *Depdc5*$^{+/-}$ mice were treated with successive pentylentetrazol doses (PTZ, 10 mg/kg every 10 min, until provocation of a tonic-clonic seizure), they displayed a significantly lower threshold to tonic-clonic seizures than *Depdc5*$^{+/+}$ littermates (p=0.039, Student's *t*-test, **Fig. 2E**).

mTOR activation in constitutive and acutely Depdc5 deficient primary neurons

To investigate mTOR activity resulting from the constitutive and acute down-regulation of *Depdc5*, we compared the extent of S6 protein phosphorylation (pS6) in *Depdc5*$^{+/+}$ and *Depdc5*$^{+/-}$ neurons or in wild type neurons treated with sh-scrambled (*Depdc5*^{Scr}) and sh3 (*Depdc5*^{KD1}) RNAs by immunoblotting (**Fig. 3A,B**). While constitutive *Depdc5*$^{+/-}$ neurons did not present an overt increase of the pS6/S6 ratio compared to *Depdc5*$^{+/+}$ (n=5, p>0.05, Student's *t*-test), *Depdc5*^{KD1} neurons displayed a ≈ 50% increase in pS6 levels with respect to *Depdc5*^{Scr} neurons (n=4, p=0.012, Student's *t*-test) (**Fig. 3A,B**). Since ectopic, pS6-positive enlarged neurons are a hallmark of FCD type 2 patients, we immunostained neuronal cultures with an anti-pS6 antibody (**Fig. 3C,E**). In agreement with biochemical analyses, *Depdc5*^{KD1} neurons displayed an increased pS6/S6 fluorescence intensity ratio (p=0.042, Student's *t*-test), accompanied by a significant increase in soma size (≈15%; p=0.013, Student's *t*-test) compared to *Depdc5*^{Scr} neurons, confirming that the associated mTORC1 hyperactivation triggers morphological changes *in vitro* (**Fig. 3D,F**).

Increased complexity of dendritic arborization in Depdc5-deficient neurons

To assess potential neurodevelopmental changes due to Depdc5 down-regulation, we next examined neurite elongation and branching by Sholl analysis in primary neurons prepared from *Depdc5*$^{+/+}$ and *Depdc5*$^{+/-}$ littermates, as well as in primary cortical neurons nucleofected with either

scr or sh3 RNAs (**Fig. 4**). In *Depdc5*$^{+/-}$ neurons, the number of intersections at distances between 90 and 110 µm from the cell body was significantly higher than in *Depdc5*$^{+/+}$ neurons (**Fig. 4A,B**), revealing an increase in neurite complexity (p=0.027, Student's *t*-test; **Fig. 4C**). The increase in neurite arborization was much more pronounced in *Depdc5*^{KD1} neurons, with a much higher number of intersections at distances between 80 and 150 µm from the cell body, resulting in a significant increase in the area under the Sholl curve when compared to *Depdc5*^{Scr} neurons and control neurons (p=0.025 and p=0.03, *Depdc5*^{Scr} and *Ctrl*, respectively, vs *Depdc5*^{KD1}; one-way ANOVA; **Fig. 4D-F**). No significant differences were detected between *Depdc5*^{Scr} and non-nucleofected controls, excluding any adverse effect of the Scr construct. These results confirm that reduction of Depdc5 levels affects neuronal development by increasing neurite outgrowth and branching.

Excitatory synaptic transmission is increased in Depdc5-deficient neurons

Imbalance between excitatory and inhibitory synaptic transmission is assumed to be at the basis of most epileptic phenotypes (Stafstrom, 2014; Bozzi et al., 2018). Thus, we asked whether constitutive or acute Depdc5 deficiency alters excitatory synaptic transmission *in vitro*. We performed electrophysiological recordings of mEPSCs in 14 DIV cortical neurons from *Depdc5*$^{+/+}$ and *Depdc5*$^{+/-}$ mice, as well as in 14 DIV wild type neurons treated with sh-scrambled (*Depdc5*^{Scr}) and sh3 (*Depdc5*^{KD1}) RNAs (**Fig. 5A,B**, respectively). While no changes in frequency, amplitude and kinetics of mEPSCs were observed in *Depdc5*$^{+/-}$ neurons (**Fig. 5C; Fig. S3A,C**), *Depdc5*^{KD1} neurons showed a 4-fold increase in mEPSC frequency (p=0.0002, Student's *t*-test), together with significant increases in amplitude (p=0.001, Mann-Whitney's *U*-test) and total charge (p= 0.002, Student's *t*-test) of the mEPSCs with respect to *Depdc5*^{Scr} controls (**Fig. 5D; Fig. S3B,D**).

To ascertain whether the changes in mEPSC frequency were attributable to variations in synaptic density, the distribution of excitatory synapses unambiguously identified by double immunolabeling for the pre/postsynaptic markers vGlut1 and Homer1 was investigated. In agreement with the electrophysiological data, no significant changes in synaptic density were detected in *Depdc5*$^{+/-}$ neuronal networks with respect to parallel *Depdc5*$^{+/+}$ cultures (**Fig. 5E**), while a marked and significant increase in the density of excitatory synaptic synapses was observed in *Depdc5*^{KD1} neurons (p<0.0001, Student's *t*-test; **Fig. 5F**) that paralleled the increase in mEPSC frequency.

To explain the changes in mEPSC amplitude and charge observed in *Depdc5*^{KD1} neurons, the synaptic expression levels of the major AMPA receptor subunit GluA1 was investigated at Homer1-positive puncta. As expected, no changes in the GluA1 fluorescence intensity were observed in *Depdc5*$^{+/-}$ neurons with respect to *Depdc5*$^{+/+}$ neurons (**Fig. 5G**), while *Depdc5*^{KD1} neurons displayed a significant increase in GluA1 fluorescence intensity compared to *Depdc5*^{Scr} control neurons (p=0.012, Student's *t*-test; **Fig. 5H**).

Inhibitory synaptic transmission is not markedly affected in Depdc5-deficient neurons

We next investigated whether Depdc5 deficiency could also alter inhibitory synaptic transmission in *Depdc5*$^{+/+}$ and *Depdc5*$^{+/-}$ neurons, as well as in *Depdc5*^{Scr} and *Depdc5*^{KD1} neurons (**Fig. 6A,B**). As observed for excitatory transmission, no detectable changes in mIPSC frequency, amplitude, charge or kinetics was observed under conditions of chronic haploinsufficiency in *Depdc5*$^{+/-}$ neurons **(Fig. 6C; Fig. S4A,C**). mIPSC frequency was neither affected after acute silencing of Depdc5 with sh3 RNA (*Depdc5*^{KD1}), although we observed an increase in the amplitude of mIPSCs (p=0.015, Mann-Whitney's *U*-test; **Fig. 6D**). However, further analysis revealed that the overall charge of mIPSCs was unchanged, and that the effects on amplitude were attributable to an acceleration of mIPSC kinetics in *Depdc5*^{KD1} neurons that showed a reduction in both the 10-90 rise time and 80% decay time (p=0.001 and 0.042, respectively, Student's *t*-test; **Fig. S4B,D**). Thus, the accelerated kinetics of mIPSCs is likely responsible for the amplitude increase at constant transferred charge.

Further immunocytochemical analysis of the density of inhibitory identified by co-staining with the pre- and post-synaptic inhibitory markers vGAT and Gephyrin, respectively, confirmed the electrophysiological results. Indeed, no differences were observed in the density of inhibitory synapses in both *Depdc5*$^{+/-}$ or *Depdc5*^{KD1} neuronal networks when compared to the respective controls (**Fig. 6E,F**). Moreover, the expression of the $GABA_A$ β2 receptor subunit, measured as intensity of the specific immunoreactivity in Gephyrin-positive puncta, was not significantly changed in both *Depdc5*$^{+/-}$ and *Depdc5*^{KD1} neurons, confirming that the increase in mIPSC amplitude observed in *Depdc5*^{KD} neurons was not contributed by an increase in quantal size (**Fig. 6G,H**).

Depdc5 deficiency does not alter synaptic ultrastructure

Although the electrophysiological phenotype was suggesting that an increase in synapse number, rather than a change in the quantal properties of synaptic transmission, was mainly responsible for the increased excitatory strength, we assessed whether Depdc5 deficiency had any effect on synaptic ultrastructure in *Depdc5*$^{+/+}$ and *Depdc5*$^{+/-}$ neurons (**Fig. 7A**), as well as in *Depdc5*^{Scr} and *Depdc5*^{KD1} neurons (**Fig. 7B**). Analysis of synaptic contacts by TEM failed to detect major changes in synaptic ultrastructure. Indeed, morphometric analysis showed no significant changes in nerve terminal area, active zone (AZ) length, the number and density of total nerve terminal SVs and number and linear density of docked SVs in both *Depdc5*$^{+/-}$ and *Depdc5*^{KD1} neurons, as compared to the respective controls (**Fig. 7C,D**). However, a significant increase (p=0.0211, Mann-Whitney's *U*-test) in the mean area of endosomes was observed in *Depdc5*^{KD1} nerve terminals, suggesting the presence of an impaired autophagic flux (**Fig. 7D**).

Acute Depdc5-deficiency increases intrinsic excitability of principal neurons

We next investigated whether Depdc5 knockdown was associated with an increase in intrinsic excitability, in addition to the observed excitatory/inhibitory synaptic imbalance. We thus performed electrophysiological recordings in the current-clamp configuration to evaluate the passive and active properties of single cortical neurons from *Depdc5*$^{+/+}$ and *Depdc5*$^{+/-}$ mice or that had been subjected to acute silencing of Depdc5 with sh3 RNA (*Depdc5*^{KD1}). No major changes in excitability were observed from the firing rate *versus* injected current curves between *Depdc5*$^{+/-}$ and *Depdc5*$^{+/+}$ neurons, in both mean firing frequency (number of APs elicited during the 500 ms of current injection) and instantaneous firing frequency a (**Fig. 8A,C**). Similarly, no changes were observed in the basic passive properties, rheobase as well as in the threshold voltage, and AP shape parameters obtained from the phase-plane plot analysis (**Table 2**). On the contrary, *Depdc5*^{KD1} neurons displayed a significant increase in the mean firing frequency at higher levels of injected current compared to *Depdc5*^{Scr} neurons (**Fig. 8B,D**), in the absence of changes in the passive membrane properties (**Table 2**).These changes were paralleled by a significant decrease in the rheobase and by significant increases of the maximum rising slope and AP peak, as calculated from the analysis of the AP waveform, consistent with a condition of hyperexcitability induced by the acute Depdc5 depletion. No changes in both passive and active membrane properties were observed between wild type neurons transduced with the scrambled construct (*Depdc5*^{Scr}) with respect to neurons transduced with the empty lentiviral vector (**Fig. S5**).

Lower acute Depdc5 depletion with an alternative shRNA triggers a similar, but milder, phenotype

To confirm that the phenotype of *Depdc5*^{KD1} neurons was not contributed by off-target effect, and to investigate whether a milder acute downregulation of Depdc5 was still able to promote a detectable phenotype, we compared the pS6/S6 ratio in wild type neurons treated with either sh-scrambled (*Depdc5*^{Scr}) or sh4 (*Depdc5*^{KD2}) RNAs by immunoblotting. *Depdc5*^{KD2} neurons displayed a ≈ 30% increase of the pS6/S6 ratio (**Fig. 9A**; p=0.044; Student's *t*-test), suggesting that an acute depletion of ≈ 40% of the Depdc5 protein is sufficient to induce hyperactivation of the mTORC1 pathway, while a chronic constitutive depletion of the same extent did not (see Fig. 3A for comparison). Consistent with the biochemical results, significantly increased pS6/S6 fluorescence intensity ratio and enlarged soma size were observed in *Depdc5*^{KD2} neurons as compared to *Depdc5*^{Scr} (**Fig. 9B,C**; p=0.041 and p=0.004, respectively; Student's *t*-test). To verify whether a partial reduction of Depdc5 levels was still able to trigger the enhancement of excitatory transmission observed with the marked depletion obtained with sh3 (*Depdc5*^{KD1}), we recorded mEPSCs in 14 DIV *Depdc5*^{Src} and *Depdc5*^{KD2} cortical neurons (**Fig. 9D**). A significant 3-fold increase in the frequency of mEPSCs was observed in *Depdc5*^{KD2} neurons (p=0.0001, Mann-Whitney's *U*-test), in the absence of significant changes in mEPSC amplitude **(Fig. 9E**). On the

other hand, the mean and instantaneous firing frequencies were not significantly different with respect to *Depdc5*^{Scr} neurons (**Fig. 9F,G**), and no changes in both passive and active membrane properties were observed (**Table 3**), consistent with the lower Depdc5 depletion of *Depdc5*^{KD2} neurons.

Discussion

DEPDC5 mutations are emerging as a frequent cause of a broad spectrum of focal epileptic syndromes (Poduri, 2014; Baldassari et al., 2019a,b), including epilepsies associated to FCD type 2 that are characterized by dysmorphic neurons displaying enhanced mTOR activation (for reviews Marsan and Baulac 2018; Iffland and Crino 2017). Notwithstanding Depdc5 has been identified as an important component of the GATOR1 inhibitory complex (Bar-Peled et al., 2013), its neuronal profile is still poorly characterized. Since mTORC1 plays a key role in neuron somatic growth, process branching and synapse formation (Laplante and Sabatini, 2012; Lasarge and Danzer, 2014), we investigated these aspects in primary cortical cultures from either heterozygous *Depdc5*$^{+/-}$ mice or silenced for Depdc5 by RNA interference.

It was previously reported that heterozygous *Depdc5*$^{+/-}$ mice failed to replicate the main hallmarks of the human pathology, such as spontaneous seizures (Marsan et al., 2016; Hughes et al., 2017). Here we show that, although *Depdc5*$^{+/-}$ mice have a reduced epileptic threshold to PTZ, primary heterozygous neurons do not exhibit overt alterations of mTORC1 signaling and, except for a slightly increased dendritic tree development, soma size and synaptic transmission are grossly comparable to WT neurons.

Strikingly, acute silencing of Depdc5 in WT neurons by RNA interference, revealed that a ≈80% decrease in *Depdc5* mRNA is able to induce morphological defects that resemble those seen in patients with FCD consisting of mTOR-hyperactive enlarged neurons. Recent studies showed the occurrence of somatic second hit *DEPDC5* variants in resected brain samples from individuals with FCD2 (Baldassari et al. 2019b, Lee et al., 2019). The somatic variant was present only in abnormal neurons within the dysplastic area and the mutation load correlated with balloon cell and dysmorphic neuron density (Baldassari et al. 2019b; Lee et al., 2019). In addition to gene dosage, our experiments highlight the importance of the temporal dynamics of Depdc5 knockdown in triggering changes in neuronal morphology and connectivity, suggesting an important neurodevelopmental role of Depdc5. Indeed, acutely depleted neurons display both an increased complexity of neuritic arborization and altered synaptogenesis, processes in which the role of mTOR in well established (Hoeffer and Klann, 2010).

While the strong phenotype observed with an 80% Depdc5 knockdown confirms the existence of a gene-dosage effect, *Depdc5*^{KD2} neurons with a Depdc5 depletion level comparable to *Depdc5*$^{+/-}$

neurons (40-50%), displayed most of the alterations observed in *Depdc5*^{KD1}, such as hyperactivation of mTORC1 pathway, increased soma size and increased frequency of mEPSCs that were absent in constitutive *Depdc5*$^{+/-}$ neurons. The milder, but clear-cut, phenotype observed *Depdc5*^{KD2} therefore suggests that the emergence of the Depdc5-related phenotype also depends on the timing of Depdc5 depletion.

Interestingly, in our models the synaptic connectivity defect appears to affect only excitatory synapses, while inhibitory synapses develop normally. The greatly increased frequency and amplitude of mEPSCs, paralleled by increased density of excitatory synapses and expression of glutamate receptors, may generate an excitation/inhibition imbalance that triggers epileptogenesis. These results differ from previous data in the zebrafish, where *Depdc5* knockout was associated with deficits in the GABAergic systems (Swaminathan et al., 2018). Although the discrepancy could be due to the time-course of Depdc5 silencing or to species-specific differences, the overall result in both experimental models will be an E/I imbalance.

Recently, it has been shown that *Depdc5* mosaic knockout leads to growth of abnormal dendritic and local hyperexcitability of pyramidal neurons (Ribierre et al., 2018; Hu et al., 2018). Our data confirm these findings, suggesting that the hyperactivation of cortical networks can result from both increased number of excitatory synaptic connections and increased expression of postsynaptic excitatory receptors, leading to increased strength of excitatory transmission. The *Depdc5*-linked epileptogenic phenotype is also contributed by an increase in the intrinsic excitability and an enhancement of AP dynamics, consistent with what observed following mosaic inactivation of mouse *Depdc5* by in utero electroporation (Ribierre et al., 2018). These results indicate that Depdc5 depletion, together with the associated hyperactivity of the mTOR pathway, has combined effects at ion channel and synaptic levels that predominantly affect excitatory neurons, thereby leading to a severe imbalance between excitatory and inhibitory activity.

The molecular mechanism underlying these defects and their specificity for excitatory neurons is still unclear. mTOR signaling has an important role in regulating the autophagy flux (Hall, 2008; Hosokawa et al., 2009; Jung et al., 2009; Kim et al., 2011; Yu et al., 2010). Autophagy is a homeostatic process that involves the turnover of intracellular organelles and proteins through the endo-lysosomal system (Glick et al., 2010). Recently, it has been shown that deficiency in mTOR-mediated autophagy could reduce synaptic pruning (Tang et al., 2014; Kim et al., 2017). Moreover, another report suggests that autophagy mediates the internalization of glutamate receptors after chemical long-term depression (Shehata et al., 2012). Indeed, the enlargement of nerve terminal endosomes, that is consistent with the synaptic defects observed after acute Depdc5 silencing, could be mediated, at least in part, by a defective autophagy following mTOR hyperactivation. This is also in line with recent studies suggesting autophagy impairment in neurons from tuberous sclerosis complex (McMahon et al., 2012; Miyahara et al., 2013), FCD (Yasin et al., 2013; Park et

al., 2018) and, more generally, in a wide spectrum of epileptic encephalopathies (Fassio et al., 2018; Esposito et al., 2019).

Conclusions

Taken together, the data indicate that the acute and marked knockdown of Depdc5 by RNA interference leads to a solid neuronal phenotype, revealing the potential mechanism of the strong phenotype of somatic second-hit mutations in patients with FCD (Ribierre et al., 2018). Growing evidence suggests that *DEPDC5* somatic mutations are present in dysmorphic neurons and trigger FCD with mTOR hyperactivation. The data uncover a novel synaptic phenotype resulting from *Depdc5* knockdown and mTOR hyperactivity with increased excitatory strength and excitatory/inhibitory imbalance, highlighting the epileptogenic potential of its deficiency. Our results represent new insight into the *Depdc5*-related epileptogenic process and represent a starting point for further investigations aimed at identifying new targets for alternative therapeutic strategies for GATOR1-related neurological disorders.

FUNDING

The work was supported by research grants from Compagnia di San Paolo (grant number 2015-0546 to FB); European Union FP7 Integrating Project "Desire" (grant number 602531 to FB); European Union "ECMED" (grant number 642881 to FB); European Research Council (grant number 682345 to SB).

ACKNOWLEDGEMENTS

We thank the IMPC European Consortium at the Sanger Institute (UK) in the frame of the European EMMA/Infrafrontier for making available the *Depdc5* KO mouse (Allele: *Depdc5*$^{tm1a(KOMP)Wtsi}$). We thank drs. Robert A. Weinberg (Whitehead Institute for Biomedical Research, Cambridge, MA) for Addgene plasmid 8454, 8455; Thorsten Trimbuch (Charité Viral Core Facility, Berlin, Germany) for production of the lentiviruses; Anna Rocchi (Italian Institute of Technology, Genova, Italy) for advice with the selection of shRNAs; Pietro Baldelli (University of Genova, Italy) for help and advice in the electrophysiological experiments; Monica Morini, (Italian Institute of Technology, Genova, Italy) and Michele Cilli (IRCCS Ospedale Policlinico San Martino, Genova, Italy) for help in breeding the mice; Riccardo Natone, Diego Moruzzo and Arta Mehilli (Center for Synaptic Neuroscience, Istituto Italiano di Tecnologia, Genova, Italy) for assistance in maintenance of mouse colonies, genotyping assays and preparation of primary neurons, respectively.

CONFLICT OF INTEREST STATEMENT

The authors declare no competing financial interests.

AUTHOR STATEMENT FILE

Antonio De Fusco

Investigation;

Data curation;

Validation;

Visualization;

Writing - original draft.

Maria Sabina Cerullo

Investigation;

Data curation;

Validation;

Visualization;

Writing - original draft.

Antonella Marte

Investigation;

Data curation.

Caterina Michetti

Investigation;

Data curation.

Alessandra Romei

Investigation;

Validation;

Visualization.

Enrico Castroflorio

Investigation.

Stephanie Baulac

Formal analysis;

Writing - review & editing.

Fabio Benfenati

Conceptualization;

Formal analysis;

Writing - review & editing;

Project administration;

Funding acquisition.

REFERENCES

Baldassari S, Picard F, Verbeek NE, van Kempen M, Brilstra EH, Lesca G, Conti V, Guerrini R, Bisulli F, Licchetta L, Pippucci T, Tinuper P, Hirsch E, de Saint Martin A, Chelly J, Rudolf G, Chipaux M, Ferrand-Sorbets S, Dorfmüller G, Sisodiya S, Balestrini S, Schoeler N, Hernandez-Hernandez L, Krithika S, Oegema R, Hagebeuk E, Cunning B, Deckers C, Berghuis B, Wegner I, Niks E, Jansen FE, Braun K, de Jong D, Rubboli G, Talvik I, Sander V, Uldall P, Jacquemont ML, Nava C, Leguern E, Julia S, Gambardella A, d'Orsi G, Crichiutti G, Faivre L, Darmency V, Benova B, Krsek P, Biraben A, Lebre AS, Jennesson M, Sattar S, Marchal C, Nordli DR Jr, Lindstrom K, Striano P, Lomax LB, Kiss C, Bartolomei F, Lepine AF, Schoonjans AS, Stouffs K, Jansen A, Panagiotakaki E, Ricard-Mousnier L, Thevenon J, de Bellescize J, Catenoix H, Dorn T, Zenker M, Müller-Schlüter K, Brandt C, Kraus L, Polster T, Wolff M, Balci M, Rostasy K, Achaz G, Zacher P, Becher T, Cloppenborg T, Yuskaitis CJ, Weckhuysen S, Poduri A, Lemke JR, Møller RS, Baulac S. The landscape of epilepsy-related GATOR1 variants. Genet Med. 2019a Feb;21(2):398-408. doi: 10.1038/s41436-018-0060-2

Baldassari S, Ribierre T, Marsan E, Adle-Biassette H, Ferrand-Sorbets S, Bulteau C, Dorison N, Fohlen M, Polivka M, Weckhuysen S, Dorfmüller G, Chipaux M, Baulac S. Dissecting the genetic basis of focal cortical dysplasia: a large cohort study. Acta Neuropathol. 2019b Aug 23. doi: 10.1007/s00401-019-02061-5.

Baldelli P, Fassio A, Valtorta F, Benfenati F. Lack of synapsin I reduces the readily releasable pool of synaptic vesicles at central inhibitory synapses. J Neurosci. 2007 Dec 5;27(49):13520-31. doi: 10.1523/JNEUROSCI.3151-07.2007.

Bar-Peled L, Chantranupong L, Cherniack AD, Chen WW, Ottina KA, Grabiner BC, Spear ED, Carter SL, Meyerson M, Sabatini DM. A Tumor suppressor complex with GAP activity for the Rag GTPases that signal amino acid sufficiency to mTORC1. Science. 2013 May 31;340(6136):1100-6. doi: 10.1126/science.1232044.

Baulac S, Ishida S, Marsan E, Miquel C, Biraben A, Nguyen DK, Nordli D, Cossette P, Nguyen S, Lambrecq V, Vlaicu M, Daniau M, Bielle F, Andermann E, Andermann F, Leguern E, Chassoux F, Picard F. Familial focal epilepsy with focal cortical dysplasia due to DEPDC5 mutations. Ann Neurol. 2015 Apr;77(4):675-83. doi: 10.1002/ana.24368.

Bockaert J, Marin P. mTOR in Brain Physiology and Pathologies. Physiol Rev. 2015 Oct;95(4):1157-87. doi: 10.1152/physrev.00038.2014.

Bozzi Y, Provenzano G, Casarosa S. Neurobiological bases of autism-epilepsy comorbidity: a focus on excitation/inhibition imbalance. Eur J Neurosci. 2018 Mar;47(6):534-548. doi: 10.1111/ejn.13595.

Browning RA, Nelson DK. Modification of electroshock and pentylenetetrazol seizure patterns in rats after precollicular transections. Exp Neurol. 1986 Sep;93(3):546-56.

Chiappalone M, Casagrande S, Tedesco M, Valtorta F, Baldelli P, Martinoia S, Benfenati F. Opposite changes in glutamatergic and GABAergic transmission underlie the diffuse hyperexcitability of synapsin I-deficient cortical networks. Cereb Cortex. 2009 Jun;19(6):1422-39. doi: 10.1093/cercor/bhn182.

Dawson RE, Nieto Guil AF, Robertson LJ, Piltz SG, Hughes JN, Thomas PQ. Functional screening of GATOR1 complex variants reveals a role for mTORC1 deregulation in FCD and focal epilepsy. Neurobiol Dis. 2019 Oct 19;134: 104640. doi: 10.1016/j.nbd.2019.104640.

de Calbiac H, Dabacan A, Marsan E, Tostivint H, Devienne G, Ishida S, Leguern E, Baulac S, Muresan RC, Kabashi E, Ciura S. Depdc5 knockdown causes mTOR-dependent motor hyperactivity in zebrafish. Ann Clin Transl Neurol. 2018 Apr 6;5(5):510-523. doi: 10.1002/acn3.542

D'Gama AM, Woodworth MB, Hossain AA, Bizzotto S, Hatem NE, LaCoursiere CM, Najm I, Ying Z, Yang E, Barkovich AJ, Kwiatkowski DJ, Vinters HV, Madsen JR, Mathern GW, Blümcke I, Poduri A, Walsh CA. Somatic Mutations Activating the mTOR Pathway in Dorsal Telencephalic

Progenitors Cause a Continuum of Cortical Dysplasias. Cell Rep. 2017 Dec 26;21(13):3754-3766. doi: 10.1016/j.celrep.2017.11.106.

De Palma M, Naldini L. Transduction of a gene expression cassette using advanced generation lentiviral vectors. Methods Enzymol. 2002;346:514-29.

Dibbens LM, de Vries B, Donatello S, Heron SE, Hodgson BL, Chintawar S, Crompton DE, Hughes JN, Bellows ST, Klein KM, Callenbach PM, Corbett MA, Gardner AE, Kivity S, Iona X, Regan BM, Weller CM, Crimmins D, O'Brien TJ, Guerrero-López R, Mulley JC, Dubeau F, Licchetta L, Bisulli F, Cossette P, Thomas PQ, Gecz J, Serratosa J, Brouwer OF, Andermann F, Andermann E, van den Maagdenberg AM, Pandolfo M, Berkovic SF, Scheffer IE. Mutations in *DEPDC5* cause familial focal epilepsy with variable foci. Nat Genet. 2013 May;45(5):546-51. doi: 10.1038/ng.2599.

Esposito A, Falace A, Wagner M, Gal M, Mei D, Conti V, Fiscano T, Aprile D, Cerullo MS, De Fusco A, Giovedì S, Seibt A, Magen D, Polster T, Eran A, Stanton SL, Fiorillo C, Ravid S, Mayatepek E, Hafner H, Wortmann S, Levanon EY, Marini C, Mandel H, Benfenati F, Distelmaier F, Fassio A, Guerrini R. Biallelic DMXL2 mutations impair autophagy and cause Ohtahara syndrome with progressive course. Brain. 2019 Dec 1;142(12):3870-3891. doi: 10.1093/brain/awz326.

Fassio A, Esposito A, Kato M, Saitsu H, Mei D, Marini C, Conti V, Nakashima M, Okamoto N, Olmez Turker A, Albuz B, Semerci Gündüz CN, Yanagihara K, Belmonte E, Maragliano L, Ramsey K, Balak C, Siniard A, Narayanan V; C4RCD Research Group, Ohba C, Shiina M, Ogata K, Matsumoto N, Benfenati F, Guerrini R. De novo mutations of the ATP6V1A gene cause developmental encephalopathy with epilepsy. Brain. 2018 Jun 1;141(6):1703-1718. doi: 10.1093/brain/awy092.

Glick D, Barth S, Macleod KF. Autophagy: cellular and molecular mechanisms. J Pathol. 2010 May;221(1):3-12. doi: 10.1002/path.2697.

Hall MN. mTOR-what does it do? Transplant Proc. 2008 Dec;40(10 Suppl):S5-8. doi: 10.1016/j.transproceed.2008.10.009.

Hoeffer CA, Klann E. mTOR signaling: at the crossroads of plasticity, memory and disease. Trends Neurosci. 2010 Feb;33(2):67-75. doi: 10.1016/j.tins.2009.11.003.

Hosokawa N, Hara T, Kaizuka T, Kishi C, Takamura A, Miura Y, Iemura S, Natsume T, Takehana K, Yamada N, Guan JL, Oshiro N, Mizushima N. Nutrient-dependent mTORC1 association with the

ULK1-Atg13-FIP200 complex required for autophagy. Mol Biol Cell. 2009 Apr;20(7):1981-91. doi: 10.1091/mbc.E08-12-1248.

Hu S, Knowlton RC, Watson BO, Glanowska KM, Murphy GG, Parent JM, Wang Y. Somatic Depdc5 deletion recapitulates electroclinical features of human focal cortical dysplasia type IIA. Ann Neurol. 2018 Jul;84(1):140-146. doi: 10.1002/ana.25272.

Hughes J, Dawson R, Tea M, McAninch D, Piltz S, Jackson D, Stewart L, Ricos MG, Dibbens LM, Harvey NL, Thomas P. Knockout of the epilepsy gene Depdc5 in mice causes severe embryonic dysmorphology with hyperactivity of mTORC1 signalling. Sci Rep. 2017 Oct 3;7(1):12618. doi: 10.1038/s41598-017-12574-2.

Iffland PH 2nd, Baybis M, Barnes AE, Leventer RJ, Lockhart PJ, Crino PB. DEPDC5 and NPRL3 modulate cell size, filopodial outgrowth, and localization of mTOR in neural progenitor cells and neurons. Neurobiol Dis. 2018 Jun;114:184-193. doi: 10.1016/j.nbd.2018.02.013.

Iffland PH 2nd, Crino PB. Focal Cortical Dysplasia: Gene Mutations, Cell Signaling, and Therapeutic Implications. Annu Rev Pathol. 2017 Jan 24;12:547-571. doi: 10.1146/annurev-pathol-052016-100138.

Ishida S, Picard F, Rudolf G, Noé E, Achaz G, Thomas P, Genton P, Mundwiller E, Wolff M, Marescaux C, Miles R, Baulac M, Hirsch E, Leguern E, Baulac S. Mutations of DEPDC5 cause autosomal dominant focal epilepsies. Nat Genet. 2013 May;45(5):552-5. doi: 10.1038/ng.2601.

Jung CH, Jun CB, Ro SH, Kim YM, Otto NM, Cao J, Kundu M, Kim DH. ULK-Atg13-FIP200 complexes mediate mTOR signaling to the autophagy machinery. Mol Biol Cell. 2009 Apr;20(7):1992-2003. doi: 10.1091/mbc.E08-12-1249.

Kim HJ, Cho MH, Shim WH, Kim JK, Jeon EY, Kim DH, Yoon SY. Deficient autophagy in microglia impairs synaptic pruning and causes social behavioral defects. Mol Psychiatry. 2017 Nov;22(11):1576-1584. doi: 10.1038/mp.2016.103.

Kim J, Kundu M, Viollet B, Guan KL. AMPK and mTOR regulate autophagy through direct phosphorylation of Ulk1. Nat Cell Biol. 2011 Feb;13(2):132-41. doi: 10.1038/ncb2152.

Laplante M, Sabatini DM. mTOR signaling in growth control and disease. Cell. 2012 Apr 13;149(2):274-93. doi: 10.1016/j.cell.2012.03.017.

Lasarge CL, Danzer SC. Mechanisms regulating neuronal excitability and seizure development following mTOR pathway hyperactivation. Front Mol Neurosci. 2014 Mar 14;7:18. doi: 10.3389/fnmol.2014.00018.

Lee WS, Stephenson SEM, Howell KB, Pope K, Gillies G, Wray A, Maixner W, Mandelstam SA, Berkovic SF, Scheffer IE, MacGregor D, Harvey AS, Lockhart PJ, Leventer RJ. Second-hit DEPDC5 mutation is limited to dysmorphic neurons in cortical dysplasia type IIA. Ann Clin Transl Neurol. 2019 Jul;6(7):1338-1344. doi: 10.1002/acn3.50815.

Marsan E, Baulac S. Mechanistic target of rapamycin (mTOR) pathway, focal cortical dysplasia and epilepsy. Neuropathol Appl Neurobiol. 2018 Feb;44(1):6-17. doi: 10.1111/nan.12463.

Marsan E, Ishida S, Schramm A, Weckhuysen S, Muraca C, Lecas S, Liang N, Treins C, Pende M, Roussel D, Le Van Quyen M, Mashimo T, Kaneko T, Yamamoto T, Sakuma T, Mahon S, Miles R, Leguern E, Charpier S, Baulac S. Depdc5 knockout rat: A novel model of mTORopathy. Neurobiol Dis. 2016 May;89:180-9. doi: 10.1016/j.nbd.2016.02.010.

McMahon J, Huang X, Yang J, Komatsu M, Yue Z, Qian J, Zhu X, Huang Y. Impaired autophagy in neurons after disinhibition of mammalian target of rapamycin and its contribution to epileptogenesis. J Neurosci. 2012 Nov 7;32(45):15704-14. doi: 10.1523/JNEUROSCI.2392-12.2012.

Miyahara H, Natsumeda M, Shiga A, Aoki H, Toyoshima Y, Zheng Y, Takeuchi R, Murakami H, Masuda H, Kameyama S, Izumi T, Fujii Y, Takahashi H, Kakita A. Suppressed expression of autophagosomal protein LC3 in cortical tubers of tuberous sclerosis complex. Brain Pathol. 2013 May;23(3):254-62. doi: 10.1111/j.1750-3639.2012.00634.x.

Park SM, Lim JS, Ramakrishina S, Kim SH, Kim WK, Lee J, Kang HC, Reiter JF, Kim DS, Kim HH, Lee JH. Brain somatic mutations in mTOR disrupt neuronal ciliogenesis, leading to focal cortical dyslamination. Neuron. 2018 Jul 11;99(1):83-97.e7. doi: 10.1016/j.neuron.2018.05.039.

Poduri A. DEPDC5 does it all: shared genetics for diverse epilepsy syndromes. Ann Neurol. 2014 May;75(5):631-3. doi: 10.1002/ana.24160.

Prestigio C, Ferrante D, Valente P, Casagrande S, Albanesi E, Yanagawa Y, Benfenati F, Baldelli P. Spike-Related Electrophysiological Identification of Cultured Hippocampal Excitatory and Inhibitory Neurons. Mol Neurobiol. 2019 Feb 12. doi: 10.1007/s12035-019-1506-5.

Ribierre T, Deleuze C, Bacq A, Baldassari S, Marsan E, Chipaux M, Muraca G, Roussel D, Navarro V, Leguern E, Miles R, Baulac S. Second-hit mosaic mutation in mTORC1 repressor DEPDC5 causes focal cortical dysplasia-associated epilepsy. J Clin Invest. 2018 Jun 1;128(6):2452-2458. doi: 10.1172/JCI99384.

Scheffer IE, Heron SE, Regan BM, Mandelstam S, Crompton DE, Hodgson BL, Licchetta L, Provini F, Bisulli F, Vadlamudi L, Gecz J, Connelly A, Tinuper P, Ricos MG, Berkovic SF, Dibbens LM. Mutations in mammalian target of rapamycin regulator DEPDC5 cause focal epilepsy with brain malformations. Ann Neurol. 2014 May;75(5):782-7. doi: 10.1002/ana.24126.

Shehata M, Matsumura H, Okubo-Suzuki R, Ohkawa N, Inokuchi K. Neuronal stimulation induces autophagy in hippocampal neurons that is involved in AMPA receptor degradation after chemical long-term depression. J Neurosci. 2012 Jul 25;32(30):10413-22. doi: 10.1523/JNEUROSCI.4533-11.2012.

Skarnes WC, Rosen B, West AP, Koutsourakis M, Bushell W, Iyer V, Mujica AO, Thomas M, Harrow J, Cox T, Jackson D, Severin J, Biggs P, Fu J, Nefedov M, de Jong PJ, Stewart AF, Bradley A. A conditional knockout resource for the genome-wide study of mouse gene function. Nature. 2011 Jun 15;474(7351):337-42. doi: 10.1038/nature10163.

Stafstrom CE. Recognizing Seizures and Epilepsy: Insights from Pathophysiology. In Epilepsy. Wiley Blackwell. 2014. p. 1-9. doi: 10.1002/9781118456989.ch1.

Stewart SA, Dykxhoorn DM, Palliser D, Mizuno H, Yu EY, An DS, Sabatini DM, Chen IS, Hahn WC, Sharp PA, Weinberg RA, Novina CD. Lentivirus-delivered stable gene silencing by RNAi in primary cells. RNA. 2003 Apr;9(4):493-501. doi: 10.1261/rna.2192803.

Swaminathan A, Hassan-Abdi R, Renault S, Siekierska A, Riché R, Liao M, de Witte PAM, Yanicostas C, Soussi-Yanicostas N, Drapeau P, Samarut É. Non-canonical mTOR-Independent-Role of DEPDC5 in Regulating GABAergic Network Development. Curr Biol. 2018 Jun 18;28(12):1924-1937.e5. doi: 10.1016/j.cub.2018.04.061.

Tang G, Gudsnuk K, Kuo SH, Cotrina ML, Rosoklija G, Sosunov A, Sonders MS, Kanter E, Castagna C, Yamamoto A, Yue Z, Arancio O, Peterson BS, Champagne F, Dwork AJ, Goldman J, Sulzer D. Loss of mTOR-dependent macroautophagy causes autistic-like synaptic pruning deficits. Neuron. 2014 Sep 3;83(5):1131-43. doi: 10.1016/j.neuron.2014.07.040.

Valente P, Lignani G, Medrihan L, Bosco F, Contestabile A, Lippiello P, Ferrea E, Schachner M, Benfenati F, Giovedì S, Baldelli P. Cell adhesion molecule L1 contributes to neuronal excitability regulating the function of voltage-gated Na+ channels. J Cell Sci. 2016 May 1;129(9):1878-91. doi: 10.1242/jcs.182089.

Yasin SA, Ali AM, Tata M, Picker SR, Anderson GW, Latimer-Bowman E, Nicholson SL, Harkness W, Cross JH, Paine SM, Jacques TS. mTOR-dependent abnormalities in autophagy characterize human malformations of cortical development: evidence from focal cortical dysplasia and tuberous sclerosis. Acta Neuropathol. 2013 Aug;126(2):207-18. doi: 10.1007/s00401-013-1135-4.

Yu L, McPhee CK, Zheng L, Mardones GA, Rong Y, Peng J, Mi N, Zhao Y, Liu Z, Wan F, Hailey DW, Oorschot V, Klumperman J, Baehrecke EH, Lenardo MJ. Termination of autophagy and reformation of lysosomes regulated by mTOR. Nature. 2010 Jun 17;465(7300):942-6. doi: 10.1038/nature09076.

Yuskaitis CJ, Jones BM, Wolfson RL, Super CE, Dhamne SC, Rotenberg A, Sabatini DM, Sahin M, Poduri A. A mouse model of DEPDC5-related epilepsy: Neuronal loss of Depdc5 causes dysplastic and ectopic neurons, increased mTOR signaling, and seizure susceptibility. Neurobiol Dis. 2018 Mar;111:91-101. doi: 10.1016/j.nbd.2017.12.010.

LEGENDS TO THE FIGURES

Fig. 1. Constitutive and shRNA-mediated knockdown of *Depdc5*

A. Representative image showing the insertion cassette of the Tm1a allele carried by *Depdc5* mouse. **B,C.** Bar plots showing *Depdc5* mRNA (**B**) and Depdc5 protein (**C**) levels in *Depdc5*$^{+/+}$, *Depdc5*$^{+/-}$ and *Depdc5*$^{-/-}$ E12.5 embryos (n=4). In **C**, a representative western bot is shown. **D,E**. Bar plots showing *Depdc5* mRNA (**D**; n=5) and Depdc5 protein (**E**; n=4) levels in wild type neurons treated with sh-scrambled (*Depdc5*^{Scr}) and sh3 (*Depdc5*^{KD1}) RNAs, respectively. In **E**, a representative western blot is shown. **F,G**. Bar plots showing *Depdc5* mRNA (**F**; n=4) and Depdc5 protein (**G**; n=4) levels in wild type neurons treated with sh-scrambled (*Depdc5*^{Scr}) and sh4 (*Depdc5*^{KD2}) RNAs, respectively. In **G**, a representative western blot is shown. Data are expressed as means ± SEM. *p<0.05; **p<0.01; ***p<0.001, Student's *t*-test (D,E,F,G) and Kruskal-Wallis ANOVA/Dunn's test (B,C).

Fig. 2. *Depdc5*$^{+/-}$ mice display alterations in the cortex architecture associated with lowered seizure threshold

A. Representative confocal cortical reconstructions of frontal (*left*) and somatosensory (*right*) cortices of *Depdc5*$^{+/+}$ and *Depdc5*$^{+/-}$ mice stained for pS6. **B.** Morphometric analysis of the number of pS6 positive cells in total cortical sections (*left*) and the number of pS6-positive cells in defined layers (*right*) of the frontal and somatosensory cortices, respectively. **C.** Representative confocal images of DAPI, vGlut1, vGAT staining and merged signals in frontal (*left*) and somatosensory (*right*) cortices of *Depdc5*$^{+/+}$ and *Depdc5*$^{+/-}$ mice. **D**. Ratio between vGlut1- and vGAT-positive puncta in the frontal (*left*) and somatosensory (*right*) cortices of *Depdc5*$^{+/+}$ and *Depdc5*$^{+/-}$ mice (n=3 mice per genotype). **E.** Seizure provocation threshold in *Depdc5*$^{+/+}$ and *Depdc5*$^{+/-}$ mice (n=8 mice per genotype) treated with progressively increasing doses of the convulsant PTZ. *p<0.05; **p<0.01; ***p<0.001, Student's *t*-test/Mann Whitney's *U*-test. Scale bars: 100 µm (A), 20 µm (C).

Fig. 3. Acute Depdc5 deficiency induces hyperactivation of the mTORC1 pathway and cell body enlargement in primary cortical neurons.

A,B. Representative western blot *(left)* and quantification (*right)* of the extent of S6 phosphorylation (pS6/total S6 ratio) in *Depdc5*$^{+/+}$ and *Depdc5*$^{+/-}$ primary cortical neurons (**A**; n=6 embryos) and in *Depdc5*^{KD1} and *Depdc5*^{Scr} neurons. (**B**; n=4 independent preparations). **C,D.** Representative confocal images of βIII-tubulin, pS6 and S6 staining (**C**) and bar plots of soma size and pS6/total S6 fluorescence intensity ratio (**D**) in primary cortical neurons from *Depdc5*$^{+/+}$ and *Depdc5*$^{+/-}$ mice (n=6 plates from 3 embryos per genotype). **E,F.** Representative confocal images of βIII-tubulin, pS6 and S6 staining (**E**) and bar plots of soma size and pS6/total S6 fluorescence intensity ratio (**F**) in *Depdc5*^{Scr} and *Depdc5*^{KD1} neurons (n=6 plates from 3 independent preparations). Data are

expressed as means ± SEM with individual experimental points. *p<0.05, Student's *t*-test. Scale bars: 10 µm.

Fig. 4. Depdc5-deficient neurons display an increased complexity of neurite arborization.
A-C. Representative reconstructions of neuronal arborization of *Depdc5*$^{+/+}$ and *Depdc5*$^{+/-}$ cortical neurons (**A**), the respective Sholl analysis (**B**) and the histogram of the area under the curve (**C**) (N=4 embryos per genotype). **D-F.** Representative reconstruction of neuronal arborization of *Depdc5*^{KD1}, *Depdc5*^{Scr} or control (Ctrl) neurons. (**D**), the respective Sholl analysis (**E**) and the histogram of the area under the curve (**F**) (n=4 independent preparations). At least 10 neurons per preparation were analyzed. Data are expressed as means ± SEM with individual experimental points. *p<0.05; **p<0.001; ***p<0.001, *Depdc5*$^{+/+}$ *vs Depdc5*$^{+/-}$ or *Depdc5*^{Scr} *vs Depdc5*^{KD1}; $^{\#\#}$p<0.01, *Ctrl vs Depdc5*^{KD1}; Student's *t*-test or One-Way ANOVA (C,F) and ANOVA for repeated measures (B,E).

Fig. 5. Acute *Depdc5* silencing increases excitatory synaptic transmission.
A,B. Representative traces of mEPSCs recorded in *Depdc5*$^{+/+}$ and *Depdc5*$^{+/-}$ (**A**) or in *Depdc5*^{KD1} and *Depdc5*^{Scr} (**B**) cortical neurons. **C.** Mean frequency and amplitude of mEPSCs in *Depdc5*$^{+/+}$ (n=17) and *Depdc5*$^{+/-}$ (n=15) neurons (*upper panels*) and the respective mEPSC cumulative curves of inter-event interval and amplitude distributions *(lower panels)*. **D.** Mean frequency and amplitude of mEPSCs in *Depdc5*^{Scr} (n=16) and *Depdc5*^{KD1} (n=19) neurons (*upper panels*) and the respective cumulative curves of mEPSC inter-event interval and amplitude distributions *(lower panels)*. The reported cumulative curves are the average of individual cumulative curves. **E.** Representative confocal images of Homer1 and vGlut1 immunoreactivities (*left*) with the highlighted colocalization puncta (*bottom panels*) and quantification of the linear density of excitatory synaptic boutons (*right*) in *Depdc5*$^{+/+}$ and *Depdc5*$^{+/-}$ neurons. **F.** Representative confocal images of Homer1 and vGlut1 immunoreactivities in tGFP-positive processes (*left*) with the highlighted colocalization puncta (*bottom panels*) and quantification of the linear density of excitatory synaptic boutons (*right*) in *Depdc5*^{Scr} and *Depdc5*^{KD1} neurons. Excitatory synapses were identified as double-positive puncta for the pre/post-synaptic markers vGlut1 and Homer1. **G.** Representative confocal images of Homer1 and GluA1 immunoreactivities (*left*) and quantification of the fluorescence intensity (*right*) of the GluA1 AMPA receptor subunit at excitatory synaptic boutons in *Depdc5*$^{+/+}$ and *Depdc5*$^{+/-}$ neurons. **H**. Representative confocal images of Homer1 and GluA1 immunoreactivities in tGFP-positive processes (*left*) and quantification of the fluorescence intensity (*right*) of the GluA1 AMPA receptor subunit at excitatory synaptic boutons in *Depdc5*^{Scr} and *Depdc5*^{KD1} neurons. All measurements were taken from n=3 independent preparations. For histology, dendrites from at least 10 neurons per each preparation were analyzed. Data are expressed as box plots. *p<0.05; **p<0.01; ***p<0.001; ****p<0.0001, Student's *t*-test/Mann Whitney's *U*-test. Scale bars: 10 µm.

Fig. 6. Acute *Depdc5* silencing increases the amplitude, but not the frequency, of mIPSCs.
A,B. Representative traces of mIPSCs recorded in *Depdc5*$^{+/+}$ and *Depdc5*$^{+/-}$ (**A**) or in *Depdc5*^{Scr} and *Depdc5*^{KD1} (**B**) cortical neurons. **C.** Mean frequency and amplitude of mIPSCs in *Depdc5*$^{+/+}$ (n=12) and *Depdc5*$^{+/-}$ (n=12) neurons (*upper panels*) and the respective cumulative curves of mIPSC inter-event interval and amplitude distributions *(lower panels)*. **D.** Mean frequency and amplitude of mIPSCs in *Depdc5*^{Scr} (n=18) and *Depdc5*^{KD1} (n=18) neurons (*upper panels*) and the respective mIPSC cumulative curves of inter-event interval and amplitude distributions *(lower panels)*. The reported cumulative curves are the average of individual cumulative curves. **E.** Representative confocal images of Gephyrin and vGAT immunoreactivities (*left*) with the highlighted colocalization puncta (*bottom panels*) and quantification of the linear density of inhibitory synaptic boutons (*right*) in *Depdc5*$^{+/+}$ and *Depdc5*$^{+/-}$ neurons. **F.** Representative confocal images of Gephyrin and vGAT immunoreactivities in tGFP-positive processes (*left*) with the highlighted colocalization puncta (*bottom panels*) and quantification of the linear density of inhibitory synaptic boutons (*right*) in *Depdc5*^{Scr} and *Depdc5*^{KD1} neurons. Inhibitory synapses were identified as double-positive puncta for the pre/post-synaptic markers vGAT and Gephyrin. **G.** Representative confocal images of Gephyrin and $GABA_A$ β2 receptor subunit immunoreactivities (*left*) and quantification of the fluorescence intensity (*right*) of the $GABA_A$ β2 receptor subunit at inhibitory synaptic boutons in *Depdc5*$^{+/+}$ and *Depdc5*$^{+/-}$ neurons. **H**. Representative confocal images of Gephyrin and $GABA_A$ β2 receptor subunit immunoreactivities in tGFP-positive processes (*left*) and quantification of the fluorescence intensity (*right*) of the $GABA_A$ β2 receptor subunit at inhibitory synaptic boutons in *Depdc5*^{Scr} and *Depdc5*^{KD1} neurons. All measurements were taken from n=3 independent preparations. For histology, dendrites from at least 10 neurons per each preparation were analyzed. Data are expressed as box plots. *p<0.05, Student's *t*-test/Mann Whitney's *U*-test. Scale bars: 10 µm.

Fig. 7. Acute *Depdc5* silencing increases the size of nerve terminal endosomes without affecting the synaptic ultrastructure.
A,B. Representative TEM micrographs showing synaptic morphology of *Depdc5*$^{+/+}$ and *Depdc5*$^{+/-}$ primary neurons (**A**), and *Depdc5*^{Scr} and *Depdc5*^{KD1} neurons (**B**). **C,D.** Histograms showing morphometric analysis of synapses from *Depdc5*$^{+/+}$ and *Depdc5*$^{+/-}$ neurons (**C**) and *Depdc5*^{Scr} and *Depdc5*^{KD1} neurons (**D**) for the following parameters: total SV number, SV density, docked SV number, docked SVs/AZ, endosome density and mean endosome area. Nerve terminal areas (means ± SEM) were: *Depdc5*$^{+/+}$, 0.811 ± 0.211; *Depdc5*$^{+/-}$, 0.832 ± 0.397; *Depdc5*^{Scr}, 0.741 ± 0.280; *Depdc5*^{KD1}, 0.652 ± 0.219. AZ lengths (means ± SEM) were: *Depdc5*$^{+/+}$, 0.496 ± 0.142;

Depdc5$^{+/-}$, 0.427 ± 0.104; *Depdc5*^{Scr}, 0.410 ± 0.110; *Depdc5*^{KD1}, 0.367 ± 0.064. All measurements were taken from 3 independent preparations. At least 10 synapses per each preparation were analyzed. Data are expressed as box plots. *p<0.05, Student's *t*-test. Scale bars: 0.2 µm and 0.05 µm (zoomed pictures).

Fig. 8. Acute *Depdc5* silencing increases intrinsic excitability.

A,B. Representative recordings of action potentials induced by the injection of 280 pA for 500 ms (*upper panels*) and representative phase-plane plots of the first action potential in the train (*lower panels*) in *Depdc5*$^{+/+}$ and *Depdc5*$^{+/-}$ neurons (**A**) and in *Depdc5*^{Scr} and *Depdc5*^{KD1} neurons (**B**). **C.** Mean number of APs evoked by the 500 ms current step in *Depdc5*$^{+/+}$ (n=22) and *Depdc5*$^{+/-}$ (n=22) primary neurons *(left)* and instantaneous frequency of APs *(right).* **D.** Mean number of APs evoked by the 500 ms current step in *Depdc5*^{Scr} (n=40) and *Depdc5*^{KD1} (n=31) neurons *(left*) and instantaneous frequency of APs *(right).* All measurements were taken from 3 independent preparations. Data are expressed as means ± SEM. *p<0.05, ANOVA for repeated measures.

Fig. 9. Lower Depdc5 depletion with an alternative shRNA triggers a similar, but milder, phenotype.

A. Representative Western Blot images (*up*) and bar plot (*down*) showing the phosphorylated S6/total S6 ratio in wild type neurons treated with sh-scrambled (*Depdc5*^{Scr}; n=4) and sh4 (*Depdc5*^{KD2}; n=4) RNAs, respectively. **B,C.** Representative immunofluorescence images **(B)** and bar plots (**C**) showing soma size and the pS6/total S6 fluorescence intensity ratio in *Depdc5*^{KD2} (n=6) and *Depdc5*^{Scr} (n=6) neurons. **D.** Representative traces of mEPSCs recorded from *Depdc5*^{Scr} and *Depdc5*^{KD2}. **E.** Box plot showing mEPSCs frequency (*left*) and amplitude (*right*) recorded in *Depdc5*^{KD2} (n=15) and *Depdc5*^{Scr} (n=17) with the respective cumulative distributions. The reported cumulative curves are the average of individual cumulative curves. **F.** Representative recordings of action potentials (*upper panels*) induced by the injection of 260 pA for 500 ms in *Depdc5*^{Scr} and *Depdc5*^{KD2} neurons and representative phase-plane plots of the first action potential in the train (*lower panels*) in *Depdc5*^{Scr} and *Depdc5*^{KD2} neurons. **G.** Mean number of APs evoked by the 500 ms current step in *Depdc5*^{Scr} (n=14) and *Depdc5*^{KD2} (n=12) neurons (*left*) and the instantaneous AP frequency (*right*). All measurements were taken from n=3 independent preparations. Data are shown either as box plots (E) or as means ± SEM (A,C,G). *p<0.05, **p<0.01, Mann Whitney's *U*-test.

Table 1. Passive and active properties of Depdc5$^{+/+}$ and Depdc5$^{+/-}$ primary cortical neurons

Parameters	*V_{rest} (mV)*	*C_{in} (pF)*	*R_{in} (MΩ)*	*Rheobase (pA)*	*V_{thr} (mV)*	*Max rising slope (mV/ms)*	*Half-width (ms)*	*AP peak (mV)*	*Max repol. slope (mV/ms)*	*Phase slope (ms^{-1})*
Depdc5$^{+/+}$	- 53.41±1.55 (n=22)	40.97 ± 3.39 (n=25)	201.8±16.25 (n=22)	213.6±9.03 (n=22)	- 30.46±1.69 (n=22)	101.4±7.3 (n=22)	1.69±0.12 (n=22)	25.17±2.20 (n=22)	- 28.57±1.96 (n=22)	10.45±0.71 (n=22)
Depdc5$^{+/-}$	- 52.55± 1.42 (n=25)	34.91±1.79 (n=27)	208.1±17.48 (n=25)	198.2±11.89 (n=25)	- 29.61±1.54 (n=25)	119.8±14.2 (n=25)	1.42±0.10 (n=25)	27.07±2.27 (n=25)	- 32.29±2.69 (n=25)	10,55±0,65 (n=25)
p	0,68	0.28	0.79	0.30	0.71	0.74	0.31	0.55	0.27	0.92

Data are expressed as means ± SEM. The number of replicates is indicated. No significant differences were detected (Student's *t*-test/Mann-Whitney's *U* test).

Table 2. Passive and active properties of Depdc5^{Scr} and Depdc5^{KD1} primary cortical neurons

Parameters	*V_{rest} (mV)*	*C_{in} (pF)*	*R_{in} (MΩ)*	*Rheobase (pA)*	*V_{thr} (mV)*	*Max rising slope (mV/ms)*	*Half-width (ms)*	*AP peak (mV)*	*Max repol. Slope (mV/ms)*	*Phase slope (ms^{-1})*
Depdc5^{Scr}	- 53.00±1.39 (n=40)	51.88 ± 4.97 (n=14)	264.4±15.28 (n=40)	160.3 ±10.26 (n=40)	- 28.61±1.04 (n=40)	67.16± 6.85 (n=40)	2.71±0.23 (n=40)	22.70±1.73 (n=40)	-20.14±1.73 (n=40)	7.201±0,48 (n=40)
Depdc5^{KD1}	- 50.84±2.11 (n=31)	42.92 ± 3.82 (n=19)	255.2 ±15.00 (n=31)	133.5 ± 7.80 (n=31)	- 29.99±1.13 (n=31)	95.89±11.16 (n=31)	2.101±0.13 (n=31)	30.29±2.63 (n=31)	- 26.50±3.11 (n=31)	8.705±0.69 (n=31)
p	0.39	0.16	0.84	0.04*	0.37	0.04*	0.1[illegible]	0.02*	0.09	0.22

Data are expressed as means ± SEM. The number of replicates is indicated. *p<0.05; Student's *t*-test/Mann-Whitney's *U*-test.

Table 3. Passive and active properties of Depdc5^{Scr} and Depdc5^{KD2} primary cortical neurons

Parameters	*V_{rest} (mV)*	*C_{in} (pF)*	*R_{in} (MΩ)*	*Rheobase (pA)*	*V_{thr} (mV)*	*Max rising slope (mV/ms)*	*Half-width (ms)*	*AP peak (mV)*	*Max repol. slope (mV/ms)*	*Phase slope (ms^{-1})*
Depdc5^{Scr}	-51,92±1,55 (n=13)	44.61± 2.30 (n=13)	246,2±17.41 (n=13)	187.7±18.85 (n=13)	-32,63±1.08 (n=13)	76.29±7.13 (n=13)	2.25±0.10 (n=13)	26.30±3.17 (n=13)	-24.71±1.51 (n=13)	8.28±0.53 (n=13)
Depdc5^{KD2}	- 53,75±1.64 (n=12)	41.33±3.16 (n=12)	225.0±1.,94 (n=12)	187.5±13.38 (n=12)	-35.65±1.19 (n=12)	87.23±8.70 (n=12)	1.92±0.09 (n=12)	24.93±2.82 (n=12)	- 26.45±2.45 (n=12)	9.92±0194 (n=12)
p	0.42	0.16	0.40	0.99	0.07	0.37	0.03*	0.75	0.55	0.14

Data are expressed as means ± SEM. The number of replicates is indicated. *p<0.05; Student's *t*-test.

Graphical abstract

Highlights:

- Acute *Depdc5* knockdown leads to a robust neuronal and synaptic phenotype
- *Depdc5* knockdown increases neuronal soma size and dendritic arborization
- *Depdc5* knockdown alters synaptic connectivity
- *Depdc5* knockdown induces an excitation/inhibition imbalance at the synaptic level
- The hyperexcitability of excitatory neurons further increases excitatory strength